

# High mass X-ray binaries in the SMC: the luminosity function

P. Shtykovskiy<sup>1,2</sup> <sup>★</sup> and M. Gilfanov<sup>2,1</sup> <sup>★</sup>

<sup>1</sup>Space Research Institute, Russian Academy of Sciences, Profsoyuznaya 84/32, 117997 Moscow, Russia

<sup>2</sup>Max-Planck-Institute für Astrophysik, Karl-Schwarzschild-Str. 1, D-85740 Garching bei München, Germany

Accepted. Received; in original form

## ABSTRACT

We study population of compact X-ray sources in the Small Magellanic Cloud using the archival data of XMM-Newton observatory. The total area of the survey is  $\approx 1.5$  square degrees with the limiting sensitivity of  $\approx 10^{-14}$  erg/s/cm<sup>2</sup>, corresponding to the luminosity of  $\approx 4.3 \cdot 10^{33}$  erg/s at the SMC distance. Out of  $\sim 150$  point sources detected in the 2–8 keV energy band,  $\sim 3/4$  are background CXB sources, observed through the SMC. Based on the properties of the optical and near-infrared counterparts of the detected sources we identified likely HMXB candidates, and sources, whose nature is uncertain, thus, providing a lower and upper limits on the luminosity distribution of HMXBs in the observed part of the SMC.

The observed number of HMXBs is consistent with the prediction based on SFR estimates derived from the supernovae frequency and analysis of color-magnitude diagrams of the stellar population. If, on the contrary, the true value of the SFR is better represented by FIR, H<sub>α</sub> and UV based estimators, then the abundance of HMXBs in the SMC may significantly (by a factor of as much as  $\sim 10$ ) exceed the value derived for the Milky Way and other nearby galaxies. The shape of the observed distribution at the bright end is consistent with the universal HMXB XLF. At the faint end,  $L_X \lesssim 2 \cdot 10^{34}$  erg/sec, the upper limit on the luminosity function is consistent with while the lower limit is significantly flatter than the  $L^{-0.6}$  power law.

**Key words:** X-rays: galaxies – X-rays: binaries – stars: neutron – galaxies: individual: SMC.

## 1 INTRODUCTION

X-ray observations of the Small Magellanic Cloud (SMC) revealed a surprisingly rich population of High Mass X-ray Binaries in this close neighbour of the Milky Way (e.g. Yokogawa et al. 2000; Haberl & Pietsch 2004). At the time of writing, about 50 sources of this type have been identified in the SMC with the majority of discovered systems being Be/X-ray binaries. Existence of such a rich population of HMXBs in a nearby galaxy opens unique possibility to study properties of population of HMXBs.

As has been shown by Grimm et al. (2003), the X-ray luminosity function (XLF) of HMXBs obeys, to the first approximation, a universal power law distribution with the differential slope of  $\approx 1.6$ , whose normalization is proportional to the star formation rate of the host galaxy. The validity of this universal HMXB XLF has been established in a broad range of the star formation rates and regimes

and in the luminosity range  $\log(L_X) \gtrsim 35.5 - 36$ . Based on the ASCA observations of the Small Magellanic Cloud and on the behavior of the integrated X-ray luminosity of distant galaxies located at redshifts  $z \sim 0.3 - 1.3$  observed by Chandra in the Hubble Deep Field North, Grimm et al. (2003) tentatively suggested, that the HMXB XLF is not dramatically affected by the metallicity variations.

Study of the population of high mass X-ray binaries in the SMC is of importance for several reasons:

(i) The Magellanic Clouds are known to have a significant under-abundance of metals (Westerlund 1997). For example, the interstellar medium of the SMC has a mean metallicity 0.6 dex lower than the local ISM, the [Fe/H] of young objects (age  $< 0.6$  Gyr) in the SMC is 0.5 dex lower than in the solar vicinity (Westerlund 1997). The effects of the metallicity variations on the population of X-ray binaries are poorly understood. Study of the SMC, a galaxy with relatively well known chemical composition gives a unique opportunity to investigate such effects observationally.

(ii) Owing to the proximity of the SMC, the weakest sources become reachable within a moderate observing time.

<sup>★</sup> E-mail: pav\_sht@hea.iki.rssi.ru; gilfanov@mpa-garching.mpg.de

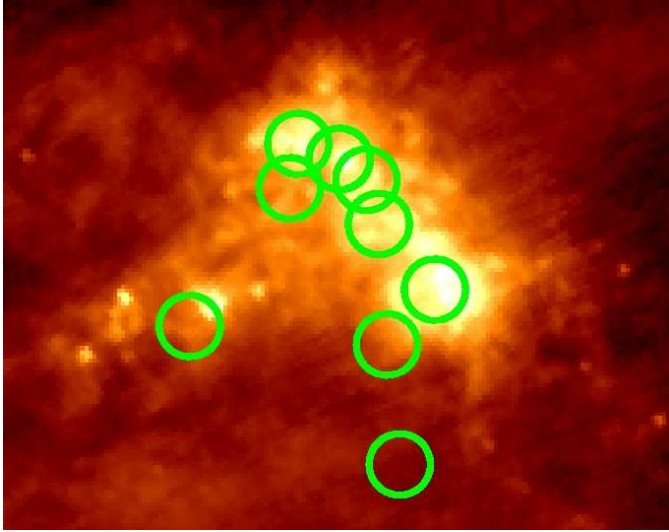


**Figure 1.** Far-infrared (IRAS,  $100\mu$ ) map of the region around the Small Magellanic Cloud. Circles show fields of view of the XMM–Newton observations used for the analysis.

Indeed, the sensitivity of a typical Chandra or XMM-Newton observation,  $\sim 10^{-14}$  erg/s/cm $^2$  corresponds to the luminosity of  $\sim 4.3 \cdot 10^{33}$  erg/s at the SMC distance. This opens the possibility to study the low luminosity end of the HMXB XLF. In addition, the proximity of the SMC allows to study the properties of its stellar population and the star formation history in details.

In the present paper we study population of X-ray binaries in the SMC based on the archival XMM-Newton data. The distance modulus of the SMC is  $m - M = 18.9$  (Westerlund 1997), corresponding to the distance of  $D \approx 60$  kpc.

The paper is structured as follows. XMM-Newton observations and data analysis are described in the section 2. In the section 3 we discuss nature of detected X-ray sources. In the section 4 we describe the HMXBs search procedure and its results. Resulting HMXBs luminosity function is presented in the section 5. The log(N)–log(S) of CXB in the direction of the SMC is presented in the section 6.

## 2 OBSERVATIONS AND DATA ANALYSIS

We have selected 9 XMM-Newton archival observations with the pointing direction towards the SMC and with sensitivity better than  $\sim \text{few} \times 10^{-14}$  erg/s/cm $^2$  in the 2–10 keV energy band. These observations are listed in Table 1. Fig.1 shows their fields of view, overlayed on the far-infrared map (IRAS,  $100\mu$ ) of the Small Magellanic Cloud.

The observations were processed with Science Analysis System (SAS) v6.0.0. After filtering out high background intervals we extracted images in the 2–8 keV energy band. This energy range was chosen to minimize the fraction of cataclysmic variables and foreground stars among detected sources, generally having softer spectra than high mass X-ray binaries. To improve the sensitivity of the survey, images from MOS1 and MOS2 detectors have been merged. If both MOS and PN data were available, we used the data having

higher sensitivity. This was determined comparing the exposure times and taking into account that the effective area of PN is  $\approx$  two times higher than the effective area of each of MOS cameras.

### 2.1 Source detection

The source detection was performed with standard SAS tasks *eboxdetect* and *emldetect*. The value of the threshold likelihood  $L$  used in *emldetect* task to accept or reject detected source was chosen as follows. We simulated a number of images with Poisson background (without sources). Each of the generated images was analyzed with the full sequence of the source detection procedures using different values of the *emldetect* threshold likelihood  $L$  and for each trial value of  $L$  the number of detected “sources” was counted. The final value of the threshold likelihood,  $L = 10.5$ , was chosen such that the total number of spurious detections was  $\lesssim 1$  per 9 images.

The obtained images were visually inspected and the source lists were manually filtered of spurious sources near bright sources and sources whose extent undoubtedly exceeded PSF size. The final merged source list contains  $\approx 150$  sources. Their flux distribution is plotted in Fig.3.

### 2.2 Energy conversion factor

The 2–8 keV source counts were converted to the 2–10 keV energy flux assuming a power law spectrum with the photon index 1 and  $N_{\text{H}}=5 \cdot 10^{20} \text{ cm}^{-2}$ . The energy conversion factors are  $\text{ecf}_{\text{MOS}}=2.95 \cdot 10^{-11} \text{ erg/cm}^2$  and  $\text{ecf}_{\text{PN}}=1.0 \cdot 10^{-11} \text{ erg/cm}^2$ . We note that, as will be shown in sec. 3.1, significant part of sources in our sample are background AGN. Therefore, in sections 3.1 and 6 (figures 2, 3 and 7) we used energy conversion factors calculated for photon index 1.7,  $\text{ecf}_{\text{MOS}}=2.27 \cdot 10^{-11} \text{ erg/cm}^2$  and  $\text{ecf}_{\text{PN}}=8.0 \cdot 10^{-12} \text{ erg/cm}^2$ , instead of values mentioned above.

### 2.3 Boresight correction

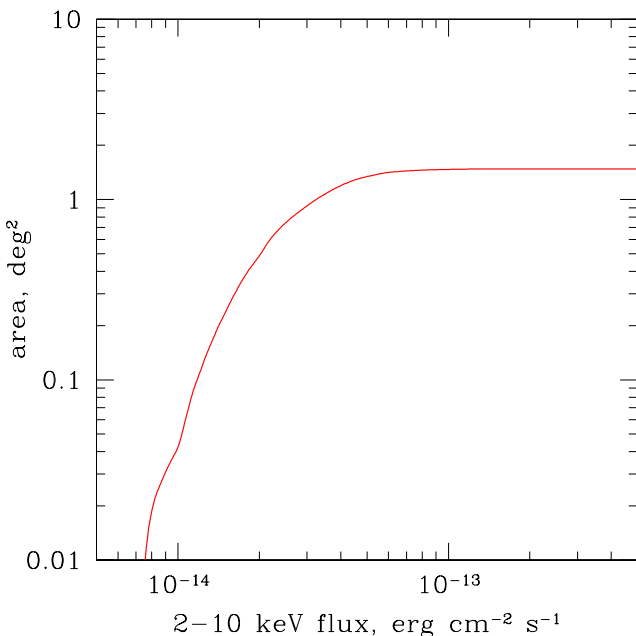
For several XMM observations we performed boresight correction using optical sources from the MCPS catalogue (Zaritsky et al. 2002). The correction was applied in case when two or more well-known sufficiently bright X-ray sources with optical counterparts were found.

### 2.4 Correction for incompleteness

Naturally, the point source detection sensitivity varies from observation to observation and, for a given observation, across the telescope field of view. The reasons of these variations are difference in the exposure times, deterioration of the point spread function of the telescope with the increase of the off-axis angle, presence of the diffuse emission and background variations. These factors affect the completeness of the survey at low fluxes. The conventional way to account for these effects without setting too high conservative completeness limit, is to calculate (using the sensitivity maps of individual observations) the survey area as a function of flux. After appropriate normalisation it represents the fraction of sources we are able to detect as a function

**Table 1.** List of XMM-Newton observations used for analysis.

Obs. ID	Target	R.A. J2000	Dec. J2000	Instrument	Exposure ksec
0135721501	1ES0102-72	16.0297	-72.0109	PN	25ks
0112880901	CF Tuc	13.3742	-74.6614	MOS1+MOS2	80ks
0110000201	IKT 18	14.9441	-72.1583	MOS1+MOS2	39ks
0110000301	IKT 23	16.3021	-72.3744	MOS1+MOS2	58ks
0110000101	IKT 5	12.3645	-73.2215	MOS1+MOS2	53ks
0084200101	SMC Pointing 1	14.1015	-72.3590	MOS1+MOS2	33ks
0084200801	SMC Pointing 8	13.7263	-73.6701	MOS1+MOS2	42ks
0011450101	SMC X-1	19.1750	-73.4381	MOS1+MOS2	102ks
0157960201	XTE J0055-727	13.9263	-72.7143	MOS2	19ks


**Figure 2.** The survey area as a function of 2–10 keV flux, calculated as described in section 2.4.

of flux, and can be used to correct the detected number of low-flux sources:

$$\left(\frac{dN}{dS}\right)_{\text{corrected}} = \frac{A_0}{A(S)} \cdot \left(\frac{dN}{dS}\right)_{\text{observed}} \quad (1)$$

where  $A(S)$  is the survey area at flux  $S$  and  $A_0$  is the total (geometrical) survey area. The corrected cumulative  $\log(N)$ – $\log(S)$  distribution can be obtained as follows:

$$N(>S) = \sum_{S_j > S} \frac{A_0}{A(S_j)}, \quad (2)$$

where  $S_j$  is the flux of the  $j$ -th source.

The flux-dependent survey area calculated as described in Shtykovskiy & Gilfanov (2005) is shown in Fig. 2. From Fig. 2 one can see that the incompleteness effects become important at fluxes  $\lesssim 10^{-13}$  erg/s/cm<sup>2</sup>. In the high flux limit, the total area of the survey equals  $A_{\text{tot}} \approx 1.48$  deg<sup>2</sup>. The flux distribution, corrected for the incompleteness effects, is plotted as the thick histogram in Fig. 3.

### 3 NATURE OF X-RAY SOURCES IN THE FIELD OF THE SMC

#### 3.1 Background and foreground sources

The total number of sources with the flux  $F_X[2–10 \text{ keV}] > 2.3 \cdot 10^{-14}$  erg/s/cm<sup>2</sup> (corresponding to the luminosity  $10^{34}$  erg/s at the SMC distance) is 151. With account for the survey incompleteness (Eq. 2) this number corresponds to  $N(> 2.3 \cdot 10^{-14}) \approx 192$  (see thick histogram in Fig. 3). According to the CXB  $\log(N) - \log(S)$  determined by Moretti et al (2003), the total number of CXB sources expected in the field of  $1.48$  deg<sup>2</sup> is  $N_{\text{CXB}} \approx 148$ . From the comparison of these numbers it is obvious that about 3/4 of sources in our sample are background AGNs.

A significantly less important source of contamination is X-ray sources associated with foreground stars in the Galaxy (no known Galactic X-ray binaries were located in the field of view of XMM observations). Foreground stars are removed by our filtering procedure, as described in section 4.

#### 3.2 Low mass X-ray binaries

Given the limiting sensitivity of the survey,  $F_X \sim (1–3) \cdot 10^{-14}$  erg/s/cm<sup>2</sup>, corresponding to the luminosity  $L_X \sim 4.3 \cdot 10^{33} – 1.3 \cdot 10^{34}$  erg/s at the SMC distance, the intrinsic SMC sources are dominated by X-ray binaries. Their total number is proportional to the stellar mass (LMXB) and star formation rate (HMXB) of the galaxy.

The total stellar mass of the SMC can be estimated from the integrated optical luminosity. According to RC3 catalog (de Vaucouleurs et al. 1991), the reddening corrected V-band magnitude of the SMC equals  $V_{T_o} \approx 1.92$ , corresponding to the total V-band luminosity of  $L_V \approx 4.6 \cdot 10^8 L_{\odot}$ . From the dereddened optical color ( $B - V$ ) <sub>$T_o$</sub>   $\approx 0.36$  (de Vaucouleurs et al. 1991) and using results of Bell & de Jong (2001), the V-band mass-to-light ratio is  $(M/L)_V \approx 0.59$  in solar units, giving the total stellar mass of the SMC  $M_* \approx 2.7 \cdot 10^8 M_{\odot}$ . For this stellar mass, using results of Gilfanov (2004), about one LMXB with luminosity  $L_X \gtrsim 10^{35}$  erg/s is expected in the entire galaxy. Such a prediction agrees with observations as no LMXB candidates are known in the SMC at present.

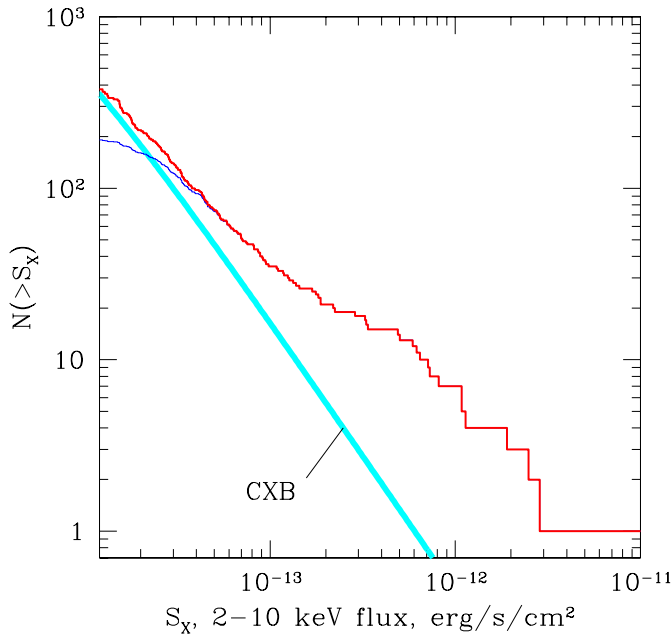


**Figure 3.** Cumulative  $\log(N)$ - $\log(S)$  distribution of detected point-like sources, excluding several known foreground stars and rotation powered pulsars (section 3). The thin and thick histograms show, respectively, the observed distribution and the distribution corrected for the incompleteness effects, as described in section 2.4. The thick grey line shows the  $\log(N)$ - $\log(S)$  of CXB sources according to Moretti et al (2003). The brightest source SMC X-1 with flux  $S_x = 6.15 \cdot 10^{-10} \text{ erg/s/cm}^2$  is situated far outside the flux range of the plot.

### 3.3 Star formation rate in the SMC

Determination of a star formation rate in the SMC, a diffuse galaxy with low opacity is a nontrivial task.

Below we compare estimates of the star formation rate in the SMC, obtained from different SFR indicators. The SFR values refer to the star formation rate of stars in the  $0.1\text{--}100 M_\odot$  range, assuming Salpeter's IMF. The discussion of results of different star formation indicators could be also found in Wilke et al. (2004) (see also discussion of the SFR in the LMC by Shtykovskiy & Gilfanov (2005)).

Wilke et al. (2004) based on ISOPHOT observations and calibration of Kennicutt (1998) obtained the star formation rate in the SMC  $\text{SFR}(\text{IR})=0.015 M_\odot/\text{yr}$ . Wilke et al. (2004), however, noted that this value underestimates the SFR of the SMC because some stellar radiation, due to low opacity of the SMC, can escape the star formation regions directly, and gave a more realistic estimate of

$$\text{SFR}(\text{IR}) = 0.05 M_\odot/\text{yr}. \quad (3)$$

With the total infrared luminosity of the SMC Wilke et al. (2004)  $L_{\text{IR}} = 3.21 \cdot 10^{41} \text{ erg/s}$  and using the equation (5) from Bell (2003) which accounts for the uncertainty mentioned above, we obtained

$$\text{SFR}(\text{IR}) = 0.044 M_\odot/\text{yr}. \quad (4)$$

Note, that this calibration should be applied extremely cautiously for such a low-luminosity galaxy (Bell 2003).

The  $\text{H}_\alpha$  luminosity-based indicators can also underesti-

mate the star formation rate in the SMC due to the reasons mentioned above. Based on  $\text{H}_\alpha$  luminosity of the SMC and applying extinction correction Kennicutt et al. (1995) estimated the star formation rate of

$$\text{SFR}(\text{H}_\alpha) = 0.044 M_\odot/\text{yr}. \quad (5)$$

Kennicutt (1991) gave an conservative upper limit of

$$\text{SFR}(\text{H}_\alpha) \lesssim 0.1 M_\odot/\text{yr}. \quad (6)$$

An SFR estimator relatively free of this uncertainty is the one based on combined UV and FIR emission. With the UV flux measured by the D 2B-Aura satellite (Vangioni-Flam et al. 1980) at  $\lambda = 1690 \text{ \AA}$  corrected for foreground extinction and uncorrected ISOPHOT FIR flux we obtain with the Kennicutt (1998) calibration

$$\text{SFR}(\text{UV} + \text{FIR}) = 0.063 M_\odot/\text{yr}. \quad (7)$$

This value is consistent with the  $\text{SFR}(\text{UV})$  derived from flux corrected for both foreground and internal extinction (Vangioni-Flam et al. 1980):

$$\text{SFR}(\text{UV, ext.corr.}) = 0.063 M_\odot/\text{yr} \quad (8)$$

Filipovic et al. (1998), from comparison of discrete radio (Parkes telescope) and X-ray (ROSAT) sources, estimated a number of SNRs in the SMC (14). From the age – radio flux density relation they estimated an SNR birth rate of one SNR in  $350 \pm 70$  yrs. We convert this value to the SFR in the mass range  $0.1\text{--}100 M_\odot$ , assuming Salpeter's IMF and taking into account that only stars with  $M \gtrsim 8 M_\odot$  can result in a radio SNR:

$$\text{SFR}(\text{SNR birth rate}) \approx 0.38_{-0.05}^{+0.10} M_\odot/\text{yr}. \quad (9)$$

Similar value has been obtained by Harris & Zaritsky (2004) who studied star formation history of the SMC fitting the color-magnitude diagrams of stellar population with theoretical isochrones:

$$\text{SFR}(\text{CMD}) \approx 0.37 M_\odot/\text{yr}. \quad (10)$$

This number corresponds to recent star formation which took place  $\sim 4\text{--}5$  Myr ago.

Thus, the SFR values derived using different star formation rate proxies can differ by the factor of as much as  $\sim$ ten. The “standart” indicators (IR, UV,  $\text{H}_\alpha$ ) result in the rather low value of  $\sim 0.05 M_\odot/\text{yr}$ , whereas the estimates based on the radio supernova rate and the analysis of the color-magnitude diagram point towards much larger star formation rates, in the  $\sim 0.3\text{--}0.4 M_\odot/\text{yr}$  range. We note, that the methods based on the analysis of the color-magnitude diagrams are generally believed to be the most reliable and accurate. As the controversy between different SFR indicators can not be resolved at present, we shall assume in the following that the true value of SFR is somewhere in the range:

$$\text{SFR}(\text{SMC}) \approx 0.05\text{--}0.4 M_\odot/\text{yr}. \quad (11)$$

### 3.4 High mass X-ray binaries

For the star formation rate of  $\text{SFR}=0.05\text{--}0.4 M_\odot \text{ yr}^{-1}$ , using HMXB-SFR relation of Grimm et al. (2003) (see also the discussion of the normalization in the HMXB-SFR calibration by Shtykovskiy & Gilfanov 2005) we predict from

~ 6 to ~ 49 HMXBs with luminosities  $\geq 10^{35}$  erg s $^{-1}$  in the whole SMC. This confirms that the population of X-ray binaries in the SMC is dominated by HMXBs.

To predict the number of HMXBs in our sample of X-ray sources, we estimate the star formation rate in the part of the SMC covered by XMM pointings from IRAS infrared maps provided by *SkyView* (McGlynn, Scollnick & White 1996). Calculating the far infrared flux according to the formula  $\text{FIR} = 1.26 \cdot 10^{-11} (2.58S_{60\mu} + S_{100\mu})$ , where FIR is flux in erg/s/cm $^2$  and  $S_\lambda$  is flux in Jy (Helou et al. 1985), and integrating the IRAS maps we obtained the total  $\text{SFR} = 0.011M_\odot/\text{yr}$ . This number is a factor of  $\sim 4.5 \div 36.4$  smaller than eq.(11) because of the uncertainties mentioned in sec. 3.3. To make it consistent with our determination of the SFR in the SMC (eq.11), we simply multiply the FIR-based values by the correction factor of  $\approx 4.5 \div 36.4$ . The thus calculated star formation rate of the part of the SMC covered by XMM observations, is:

$$\text{SFR}(\text{XMM}) \approx 0.018 \div 0.15M_\odot/\text{yr}. \quad (12)$$

With the above value of SFR we predict about  $\sim 2 \div 18$  HMXBs with luminosities  $\geq 10^{35}$  erg s $^{-1}$  in the observed part of the SMC. The error in this number accounts for uncertainty of the SFR estimate and does not include the Poisson fluctuations.

### 3.5 The Log(N)–Log(S) distribution

As demonstrated above, the population of compact X-ray sources in the SMC field is dominated by two types of sources – background AGN and high mass X-ray binaries in the SMC. Their log(N)–log(S) distributions in the flux range of interest can be described by a power law with the differential slopes  $\approx 2.5$  (CXB) and  $\approx 1.6$  (HMXBs). Due to significant difference in the slopes, their relative contributions depend strongly on the flux. At large fluxes,  $F_X \gtrsim (2\text{--}3) \cdot 10^{-13}$  erg/s/cm $^2$  ( $L_X \gtrsim 10^{35}$  erg/s) the X-ray binaries in the SMC prevail. On the contrary, in the low flux limit, e.g. near the sensitivity limit of our survey,  $F_X \sim 10^{-14}$  erg/s/cm $^2$ , the majority ( $\sim 3/4$ ) of the X-ray sources are background AGN.

This is illustrated by Fig. 3, showing the observed and corrected for incompleteness log(N)–log(S) distribution of all sources from the final source list. The corrected log(N)–log(S) distribution agrees at low fluxes with that of CXB sources. At high fluxes, there is an apparent excess of sources above the numbers predicted by the CXB sources log(N)–log(S), due to the contribution of HMXBs.

## 4 IDENTIFICATION OF HMXB CANDIDATES

To filter out contaminating background and foreground sources, we use the same filtering procedure as described by Shtykovskiy & Gilfanov (2005). It is based on the fact that optical emission from HMXBs is dominated by their optical companions, whose properties, such as absolute magnitudes and intrinsic colors are sufficiently well known.

### 4.1 Optical properties of HMXBs counterparts

High mass X-ray binaries are powered by accretion of mass lost from the massive early-type optical companion. The

mechanism of accretion could be connected either to (i) strong stellar wind from an OB supergiant (or bright giant) or (ii) equatorial circumstellar disk around Oe or Be type star (e.g. Corbet 1986; van Paradijs & McClintock 1994). In the case of Small Magellanic Cloud where the only supergiant system SMC X-1 is known at present time, the HMXBs with Be companion seem to give the main contribution (Coe et al. 2004).

Given the large number of well known high mass X-ray binaries in the SMC, the selection criteria for the optical counterparts of such systems can be determined straightforwardly. For example, Coe et al. (2004) studied the optical properties of Be/X-ray pulsars in the SMC. The majority of HMXBs with identified optical companions in their sample (32 out of 34) have apparent V-band magnitudes  $m_V = 14 \div 17$ . The exceptions are supergiant system SMC X-1 with  $m_V = 13.2$  and X-ray pulsar CXOU J010042.8–721132 with  $m_V = 18.01$  (OGLE catalogue Udalski et al. 1998) which has been previously classified by Lamb et al. (2002) as a possible anomalous X-ray pulsar (AXP).

This picture is consistent with the expectations based on the positions of possible optical counterparts on the Hertzsprung–Russel diagram, distance modulus of the SMC,  $(m - M)_0 = 18.9$  (Westerlund 1997), and foreground and intrinsic extinction towards the SMC,  $A_V \sim 0.46$  (for hot population) (Zaritsky et al. 2002). OB supergiants and bright giants (luminosity classes I–II) have absolute magnitudes  $M_V \sim -7 \div -4$ , corresponding to apparent magnitudes in the range  $m_V \sim 12.5 \div 15.5$ . The position of Be stars in the H–R diagram is close to the main sequence. Apparent magnitudes  $m_V < 17 \div 18$  correspond to spectral classes earlier than B3–B5 for main sequence stars (B5–B7 for giants). Thus we can conclude, that HMXBs in the SMC with main sequence Be optical companions have spectral classes earlier than B3–B5 (B5–B7 for giants), in agreement with expectations based on the optical properties of HMXBs in our Galaxy.

As potential optical counterparts of HMXBs belong to spectral classes earlier than  $\sim$  B3–B5, their intrinsic optical and near-infrared colors are constrained by  $B - V \lesssim -0.20$ ,  $J - K \lesssim -0.16$ . With account for the interstellar reddening, both apparent colors are expected to be  $\lesssim 0.1 \div 0.2$ . This is consistent with B–V colors of HMXBs from Coe et al. (2004) sample. In infrared part of the spectrum, however, Be stars are known to exhibit an infrared continuum excess, caused by free-free and free-bound emission within the disk (Gehrz et al. 1974). Therefore, J–K colors of Be stars can be higher than values quoted above. To avoid this uncertainty, in identification procedure we use mainly B–V colors, applying J–K identification criteria only in extreme cases (in fact we used this criteria alone only for one source).

### 4.2 Catalogs and selection criteria

We used the following optical and near-infrared catalogs:

- (i) Magellanic Clouds Photometric Survey: the SMC (MCPS) (Zaritsky et al. 2002)
- (ii) Guide Star Catalog, version 2.2.1 (GSC2.2.1) (Morrison & McLean 2001)
- (iii) The CCD survey of the Magellanic Clouds (Massey et al. 2002)

- (iv) 2-micron All Sky Survey (2MASS) (Cutri et al. 2003)
- (v) Emission-line stars and PNe in the SMC (Meyssonnier et al. 1993)
- (vi) A 2dF survey of the Small Magellanic Cloud (Evans et al. 2004)

As a first step, we cross-correlated the XMM-Newton X-ray source list with MCPS, GSC and Massey et al. (2002) optical catalogs, using search radius  $4''$  and the following selection criteria:  $12.0 < V < 18.0$ ,  $B - V < 0.6$ . If optical object was present in MCPS and either GSC or Massey et al. (2002) catalogs, the preference was given to MCPS, as it has a higher photometric accuracy (especially at low magnitudes). The color limits are higher than possible colors of HMXBs optical companions ( $B - V \lesssim 0.1 - 0.2$ ) and were chosen to account for limited photometric accuracy of optical catalogues. We found optical counterparts for 54 X-ray sources using these selection criteria.

On the second stage, we cross-correlated all X-ray sources having optical counterparts with near-infrared catalog 2MASS, catalog of Meyssonnier et al. (1993) and catalog of Evans et al. (2004) using the same search radius as before.

Then the following filtering procedure was applied.

(i) In case when source was present only in the GSC catalogue (which has rather low photometric accuracy), we applied filtering criteria based on the near infrared data. In fact, there was only one source with  $J - K \approx 1.2$  rejected by this criteria.

(ii) All X-ray sources with low X-ray-to-optical flux ratio  $F_X/F_{\text{opt}} < 10^{-3}$  were rejected. The optical flux was calculated from the V-band magnitude,  $F_{\text{opt}} = 8.0 \cdot 10^{-6} \cdot 10^{-mv/2.5} \text{ erg/s/cm}^2$ . Such low  $F_X/F_{\text{opt}} < 10^{-3}$  ratios are typical for foreground stars but not for X-ray binaries. All confirmed HMXBs in our sample have  $F_X/F_{\text{opt}} > 3 \cdot 10^{-3}$  among which  $\gtrsim 90\%$  have  $F_X/F_{\text{opt}} > 10^{-2}$ .

### 4.3 Search radius

The choice of the search radius plays a crucial role in the procedure of search for potential HMXB candidates based on their optical companions. Too small value of the search radius may lead to incompleteness of resulting HMXBs list (especially at low luminosities), while too large value may lead to a significant fraction of chance coincidences. Given the spatial density of optical stars (whose optical colors and magnitudes satisfy our selection criteria) in the MCPS catalogue, the number of detected X-ray sources and the search radius of  $4''$ , we estimate the number of chance coincidences to be  $\approx 14$ . On the other hand, a typical error on the position of a low-luminosity source is  $\sigma \approx 2''$  ( $1\sigma$  confidence). Therefore, in ideal situation with the search radius of  $4''$  we miss only  $\sim 13\%$  of low-luminosity sources. The real fraction of missed optical counterparts, however, could be somewhat higher as it was obtained assuming ideal astrometric accuracy. Our choice of the search radius is further justified in the Appendix.

### 4.4 Identification results

After the filtering, 50 X-ray sources remained in the list of potential HMXB candidates (Table 2). As follows from

sec.4.3,  $\approx 14$  of these sources can be chance coincidences. Therefore, we further split the filtered list into reliable HMXBs and the sources whose nature is less certain. We include in the list of reliable HMXB candidates only sources which have either detected X-ray pulsations or optical emission lines, or sources whose spectral class is well-determined based on their optical spectrum. The latter two identification criteria are mainly based on Meyssonnier et al. (1993) and Evans et al. (2004) catalogues.

There were 32 sources satisfying at least one of these criteria. Remaining 18 sources are considered to be sources of uncertain nature.

The resulting likely HMXBs candidates and sources of uncertain nature are listed in Table 2. All known HMXBs located in the field of view of the XMM-Newton observations are among these sources.

Comments on the individual sources:

#1: To minimize the influence of pile-up on the flux of SMC X-1, for this source we used data from EPIC PN camera operating in Small Window mode.

#17 = RXJ0049.2-7311: Optical colors consistent with HMXB nature. This source was identified with an bright  $H_{\alpha}$  object by Coe et al. (2004) and is probably associated with nearby X-ray pulsar AXJ0049-732 ( $p=9s$ ).

#34: Optical colors consistent with HMXB nature, however, infrared colors are relatively high,  $J - K = 0.97$ .

#35: Optical colors consistent with HMXB nature. Lamb et al. (2002) classified this source as a possible anomalous X-ray pulsar ( $p=8s$ ).

#38: This source is situated inside the NGC 330 stellar cluster. As a stellar density is high there, we consider the photometry to be unreliable.

#49: Optical colors consistent with HMXB nature. This source is situated in  $24''$  from source AXJ0048.2-7309. Yokogawa et al. (2003) based on the presence of emission-line object in Meyssonnier et al. (1993) catalogue within the ASCA error circle of  $40''$  (90% confidence) and X-ray spectrum classified this ASCA source as a possible Be X-ray pulsar. The position of the XMM source is inconsistent with emission-line object in Meyssonnier et al. (1993) and therefore either optical identification of ASCA source was incorrect either XMM source is unrelated to ASCA source. Therefore we consider this source as a source of uncertain nature.

### 4.5 Completeness

The completeness of the list of HMXB candidates is defined by the following factors:

(i) The completeness of the optical catalogues. The initial search for optical counterparts is based on MCPS and GSC2.2 catalogs. In general, the MCPS catalogue is thought to be complete for  $V < 20$  (Zaritsky et al. 2002). The GSC2.2 is a magnitude selected ( $V \leq 19.5$ ) subset of the GSC-II catalog (<http://www-gsss.stsci.edu/gsc/gsc2/GSC2home.htm>). The latter is complete to  $J = 21$  at high galactic latitudes (Morrison & McLean 2001).

Completeness of both catalogs is known to break down in the crowded regions. As no sensitivity maps for the optical catalogs exist, a quantitative estimate of the completeness

**Table 2.** List of HMXB candidates

#	R.A.	Dec.	$L_X$ (1) erg s <sup>-1</sup>	$m_V$	$B - V$	$F_x/F_{opt}$	id	Comments
<i>Likely HMXB candidates</i>								
1	01 17 05.2	-73 26 38	$3.8 \cdot 10^{38}$	13.2	-0.14	0.55	p, ob	SMC X-1 P=0.717s (2)
2	00 47 23.3	-73 12 28	$1.4 \cdot 10^{36}$	16.0	0.08	0.80	p	RX(AX)J0047.3-7312 P=263s (2)
3	00 51 52.3	-73 10 34	$1.1 \cdot 10^{36}$	14.5	-0.07	0.14	p,em	RXJ0051.9-7311=AXJ0051.6-7311 P=172s (2)
4	00 49 42.0	-73 23 14	$6.4 \cdot 10^{35}$	14.9	0.15	0.12	p,em	RXJ0049.7-7323=AXJ0049.5-7323 P=755.5s (2)
5	00 57 50.4	-72 07 55	$6.1 \cdot 10^{35}$	15.7	-0.05	0.26	p,em	CXOUJ005750.3-720756 P=152.3s (2)
6	00 54 55.9	-72 45 10	$5.2 \cdot 10^{35}$	15.0	-0.03	0.14	p,em	AXJ0054.8-7244 P=500s(2,3)
7	00 57 49.6	-72 02 35	$4.6 \cdot 10^{35}$	15.7	-0.12	0.19	p,em	RXJ0057.8-7202=AXJ0058-72.0 P=280.4s (2)
8	01 01 20.8	-72 11 17	$4.0 \cdot 10^{35}$	15.6	-0.19	0.15	p,em	RXJ0101.3-7211 P=455s (2)
9	01 01 52.1	-72 23 34	$4.0 \cdot 10^{35}$	14.9	-0.01	0.084	em, ob	AXJ0101.8-7223(2)
10	00 55 18.5	-72 38 52	$3.6 \cdot 10^{35}$	15.9	0.15	0.18	p	P=702s (3)
11	00 59 20.9	-72 23 15	$3.5 \cdot 10^{35}$	15.0	-0.01	0.075	p	XMMUJ005921.0-722317 P=202s (4)
12	00 50 57.3	-73 10 09	$3.3 \cdot 10^{35}$	14.4	0.08	0.040	em	RXJ0050.9-7310=AXJ0050.8-7310 (2)
13	00 50 44.6	-73 16 05	$2.9 \cdot 10^{35}$	15.5	-0.11	0.097	p,em	RXJ0050.8-7316 AXJ0051-733 P=323.2 (2)
14	01 03 13.4	-72 09 13	$2.7 \cdot 10^{35}$	14.8	-0.06	0.053	p,em	SAXJ0103.2-7209=AXJ0103.2-7209 P=345.2 (2)
15	00 58 12.4	-72 30 50	$2.0 \cdot 10^{35}$	14.9	0.11	0.038	em <sup>5</sup>	RXJ0058.2-7231 (2,5)
16	00 55 28.5	-72 10 57	$1.8 \cdot 10^{35}$	16.8	-0.12	0.21	p	CXOUJ005527.9-721058 P=34s (6)
17	00 49 13.7	-73 11 38	$1.3 \cdot 10^{35}$	16.4	0.19	0.10	em	=?(?)AXJ0049-732(P=9s) RXJ0049.2-7311 (2,7,10)
18	00 48 34.3	-73 02 31	$9.9 \cdot 10^{34}$	14.8	0.0	0.023	em, ob	RXJ0048.5-7302 (2)
19	00 54 56.4	-72 26 48	$8.1 \cdot 10^{34}$	15.3	-0.05	0.023	p,em	XTEJ0055-724 P=59s (2)
20	01 05 55.3	-72 03 51	$6.6 \cdot 10^{34}$	15.7	-0.06	0.028	em	RXJ0105.9-7203 AXJ0105.8-7203 (2)
21	01 01 37.4	-72 04 18	$6.1 \cdot 10^{34}$	16.3	-0.16	0.044	em	RXJ0101.6-7204 (2)
22	00 56 15.2	-72 37 54	$4.9 \cdot 10^{34}$	14.6	0.13	0.0075	em, ob	
23	00 57 36.1	-72 19 33	$4.8 \cdot 10^{34}$	16.0	0.01	0.027	em,p	CXOUJ005736.2-721934 P=565s (2)
24	00 57 24.0	-72 23 57	$4.0 \cdot 10^{34}$	14.7	-0.07	0.0068	ob	
25	00 49 29.9	-73 10 58	$3.5 \cdot 10^{34}$	16.2	0.2	0.023	em	=?(?)AXJ0049-732(P=9s)(2,7)
26	01 05 08.1	-72 11 48	$3.5 \cdot 10^{34}$	15.7	-0.08	0.016	em	RXJ0105.1-7211 AXJ0105-722 P=3.34s? (2)
27	01 03 37.7	-72 01 35	$3.4 \cdot 10^{34}$	14.7	-0.11	0.0055	em	RXJ0103.6-7201 (2)
28	01 19 39.0	-73 30 14	$3.3 \cdot 10^{34}$	15.9	-0.07	0.016	em	(4)
29	01 01 03.0	-72 07 01	$2.7 \cdot 10^{34}$	15.8	-0.07	0.013	em	RXJ0101.0-7206 P=304.5 (2)
30	01 00 30.3	-72 20 32	$2.1 \cdot 10^{34}$	14.6	-0.06	0.0034	em, ob	XMMUJ010030.2-722035 (2)
31	00 56 05.8	-72 21 57	$2.0 \cdot 10^{34}$	15.9	-0.04	0.097	p,em	XMMUJ005605.2-722200 P=140.1 (2)
32	00 50 47.9	-73 18 12	$8.7 \cdot 10^{33}$	15.6	0.12	0.0035	em	
<i>Sources of uncertain nature</i>								
33	00 55 34.9	-72 29 05	$2.1 \cdot 10^{35}$	14.7	-0.04	0.031		
34	00 48 18.8	-73 21 00	$1.1 \cdot 10^{35}$	16.2	0.25	0.069		
35	01 00 42.9	-72 11 32	$1.1 \cdot 10^{35}$	17.7	-0.03	0.28	p	CXOUJ010043.1-721134 AXP? P=8s (8)
36	00 54 32.2	-72 18 09	$7.2 \cdot 10^{34}$	16.6	-0.08	0.067		
37	00 54 03.6	-72 26 30	$6.6 \cdot 10^{34}$	14.9	0.01	0.014		
38	00 56 18.7	-72 28 02	$3.9 \cdot 10^{34}$	15.3	-0.40	0.012		NGC330 stellar cluster
39	01 00 37.2	-72 13 16	$2.5 \cdot 10^{34}$	16.7	-0.17	0.026		
40	00 48 33.4	-73 23 55	$2.5 \cdot 10^{34}$	17.7	0.07	0.064		
41	00 54 41.1	-72 17 20	$2.1 \cdot 10^{34}$	15.7	-0.11	0.0090		
42	00 47 19.9	-73 08 22	$2.0 \cdot 10^{34}$	17.3	0.08	0.036		
43	00 53 35.8	-72 34 24	$1.7 \cdot 10^{34}$	17.2	-0.07	0.029		
44	01 04 37.4	-72 06 30	$1.4 \cdot 10^{34}$	18.0	0.13	0.048		
45	01 00 22.9	-72 11 27	$1.2 \cdot 10^{34}$	17.0	-0.13	0.018		
46	00 48 04.0	-73 17 01	$1.2 \cdot 10^{34}$	17.0	0.21	0.016		
47	00 49 05.4	-73 14 10	$1.0 \cdot 10^{34}$	18.0	0.03	0.034		
48	01 03 28.3	-72 06 51	$1.0 \cdot 10^{34}$	16.5	-0.15	0.0086		
49	00 48 14.9	-73 10 03	$8.6 \cdot 10^{33}$	15.3	0.26	0.0025		=?(?)AXJ0048.2-7309 (2,9)
50	00 50 20.2	-73 11 17	$8.6 \cdot 10^{33}$	17.0	0.11	0.012		

(1) – 2–10 keV band, assuming distance of 60 kpc; (2) – see Haberl & Pietsch (2004) and references inside; (3) – Haberl et al. (2004); (4) – Majid et al. (2004); (5) – Edge & Coe (2003); (6) – Edge et al. (2004); (7) – Filipovic et al. (2000); (8) – Lamb et al. (2002); (9) – Yokogawa et al. (2003); (10) – Coe et al. (2004); Comments: p – source shows pulsations; em – source has Balmer emission lines in its optical spectrum (based on Meyssonnier et al. (1993) catalogue, unless otherwise is noted); ob – source is present in Evans et al. (2004) catalogue and belongs to OB spectral class;

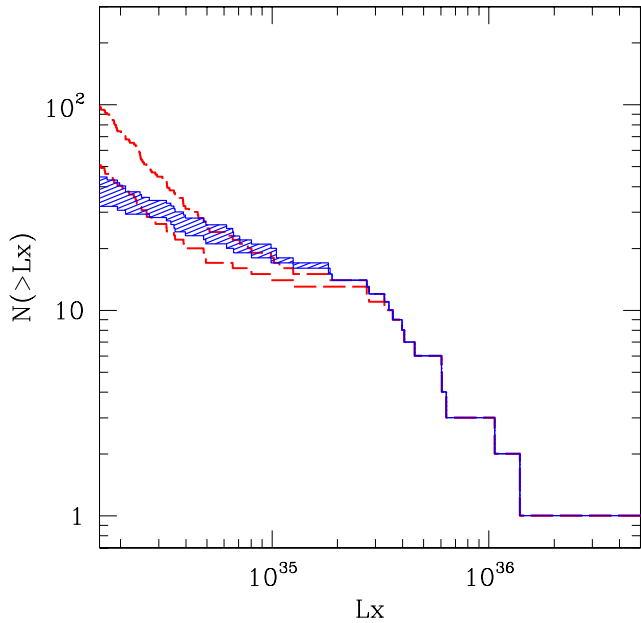


**Figure 4.** The incompleteness-corrected XLFs of HMXB candidates in the SMC obtained with two different HMXB search methods (see sec.4.6). Two solid histograms correspond to upper and lower limits on XLF obtained with search method based on the optical properties of HMXBs. Two dashed histograms correspond to upper and lower limits on XLF obtained with search method based on the X-ray hardness ratio. It is clear from this figure, that both methods give similar result for sources with luminosities  $L_X \gtrsim 2 - 3 \cdot 10^{34}$  erg/s. The brightest source SMC X-1 with luminosity  $L = 3.8 \cdot 10^{38}$  erg/s is situated outside the luminosity range of the graph.

of the initial counterpart search is impossible. However, the quoted completeness limits of both catalogs are 2 – 3 mag better than chosen threshold of 18 mag for the optical counterparts search. This suggests that the completeness of the optical catalogs is unlikely to be the primary limiting factor.

The MCPS catalogue also has “stripe-like” gaps with zero stellar density. We checked that the majority of X-ray sources do not coincide with this “gaps”. For few sources which were close or inside the gaps we used two additional catalogs: OGLE (Udalski et al. 1998) and (if OGLE had no data in this region) USNO-B (Monet et al 2003).

(ii) The efficiency of the initial search due to statistical and systematic uncertainties in the positions of X-ray and optical sources. This is probably one of the major limiting factors. As has been noted in sec 4.3, the search radius of 4'' assuming ideal astrometric quality corresponds to detection of  $\sim 87\%$  of the weakest sources, while for moderate luminosity and bright sources this fraction would be close to 100%. In Appendix we show, that in real case (i.e. with all uncertainties taken into account), with the chosen value of the search radius we miss not more than few sources.

(iii) The filtering procedure applied to the optical matches found in the initial search. This procedure is based mainly on observed optical and near-infrared properties of known HMXBs in the SMC and Milky Way. The distribution of V-band magnitudes and B-V optical colors of

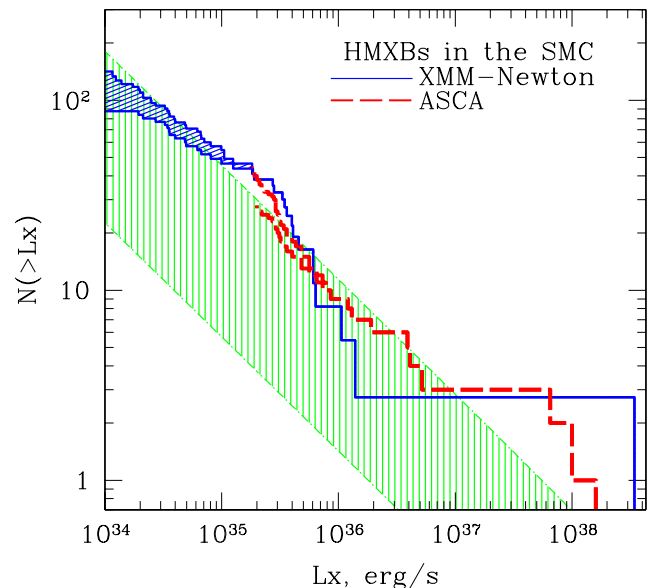


**Figure 5.** The upper and lower limits on the XLF of HMXBs in the SMC. The solid histogram shows XMM-Newton results scaled up by the factor of  $SFR_{tot}/SFR_{XMM} \approx 2.7$  according to the contribution of the XMM-Newton survey area to the total SFR of the SMC. The dashed histogram is the ASCA XLF from Yokogawa et al. (2003). The shaded area shows the luminosity distribution predicted from the “universal” HMXB XLF of Grimm et al. (2003) extrapolated towards low luminosities. Its width reflects the uncertainty of our knowledge of the SFR in the SMC, as discussed in the section 3.3.

HMXBs in the SMC have maxima far inside our filtering limits (see Fig. 6), meaning that we detect the vast majority of HMXBs unless some significantly different (and previously undetected) type of these systems exists.

Thus, we estimate the completeness of our HMXBs sample to be very high with the uncertainties in the positions of X-ray sources being the main factor of incompleteness. We note, that as this factor is flux-dependent, it affects most strongly the low-luminosity part of our sample.

#### 4.6 Comparison with other HMXB identification methods

The identification method based on the properties of optical counterparts is not the only way to identify the population of HMXBs in the background of contaminating sources. For example, Yokogawa et al. (2000) found that hardness ratios (HRs) of all known X-ray binary pulsars (XBPs) in the Magellanic Clouds fall into narrow “XBP region”,  $HR_{XBP}(\text{ASCA}) = 0.2 - 0.6$ . In order to compare these two methods, we apply selection criteria based on hardness ratio to our sample of X-ray sources.

We use XBPs selection criteria similar to those described in Yokogawa et al. (2000). The hardness ratio is defined as  $HR = (H - S)/(H + S)$ , where H and S are count rates in the 2-7 keV and 0.7-2 keV energy bands respectively. All X-ray sources with HRs corresponding to photon

indexes  $\alpha = 0.4 - 1.5$  (corresponding “XBP region” defined by Yokogawa et al. (2000)) are classified as X-ray binary pulsar candidates. X-ray sources which have slightly softer spectra,  $\alpha = 1.5 - 2.0$ , are considered as sources of uncertain nature. Higher photon indexes are untypical for HMXBs, especially for Be/X-ray binaries which seem to constitute the majority of HMXBs population in the SMC. Luminosity distributions obtained using these two methods are shown in Fig. 4.

As is clear from Fig. 4, the results of both methods agree for sources with  $L_X \gtrsim 2 - 3 \cdot 10^{35}$  erg/s, while for the low-luminosity sources the method based on hardness ratio gives significantly higher number of sources. This could be a result of large statistical uncertainty in the hardness ratios for low flux sources, leading to a “leakage” of background AGN to the XBP region. In addition, the population of highly absorbed AGN with truly hard spectra becomes important at low fluxes and compromises the simple hardness ratio based selection criteria.

## 5 POPULATION OF HMXBS IN THE SMC

### 5.1 The luminosity function of HMXBs in the SMC

The incompleteness-corrected luminosity distribution of HMXBs in the SMC is shown in Fig. 5. In order to represent the HMXB population of the entire galaxy, the observed XLF has been scaled up according to the relative contribution of the area covered by the XMM-Newton survey to the total SFR of the SMC. The upper and lower histograms below  $\sim 2 \cdot 10^{35}$  erg/sec correspond to all sources from Table 2 and to the likely HMXB candidates respectively. These two histograms provide upper and lower limits on the true X-ray luminosity function of HMXBs in the observed part of the SMC.

Fig. 5 also shows the XLF of HMXB candidates in the SMC obtained by Yokogawa et al. (2003) based on the ASCA data. The ASCA XLF refers to the entire SMC. We note that removal of the sources located outside XMM pointings does not change its shape significantly. The upper ASCA histogram in the figure corresponds to all sources from Yokogawa et al. (2003) excluding SNR, AGN and foreground stars – i.e. represents all sources which properties do not contradict to HMXB nature. The lower histogram shows the luminosity distribution of likely HMXB candidates – confirmed X-ray binary pulsars and candidates and confirmed non-pulsating HMXBs and candidates (see Yokogawa et al. 2003 for details). As is evident from the figure, the XMM-Newton and ASCA XLFs are consistent with each other. The K-S test for two distribution gives the probability of  $\sim 50 - 70\%$ .

### 5.2 Abundance of HMXBs in the SMC

The shaded area in Fig. 5 shows the universal HMXB XLF of Grimm et al. (2003) and its extrapolation towards low luminosities. The width of the shaded area reflects uncertainties in our knowledge of the star formation rate in the SMC as discussed in the section 3.3. As is clear from Fig. 5, the observed abundance of HMXBs in the SMC is consistent with

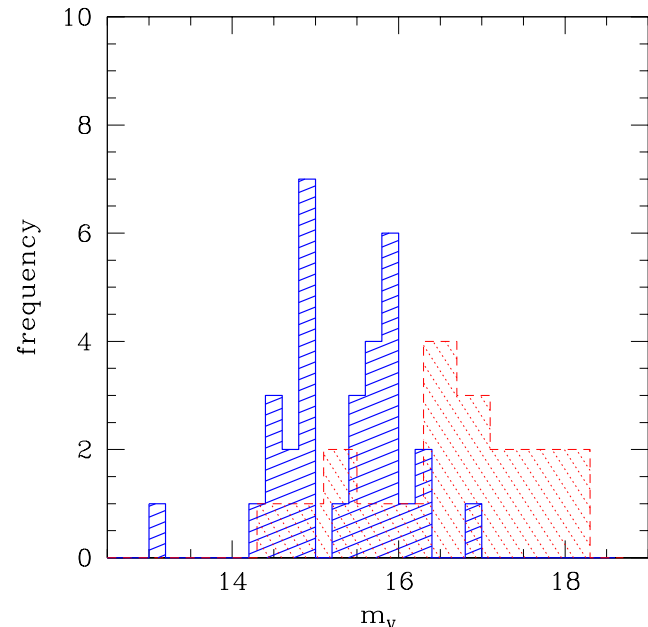


**Figure 6.** Distribution of the V-band magnitudes of the HMXB candidates in the SMC. The thick histogram corresponds to the likely HMXB candidates from the upper part of the table 2. The thin histogram corresponds to the uncertain sources from the lower part of the table 2.

the upper range of the predicted numbers, which is based on the SFR estimates derived from the supernovae rate and analysis of the stellar color-magnitude diagram. If, on the contrary, the true value of the SFR is better represented by FIR,  $H_\alpha$  and UV based estimators, then the abundance of HMXBs in the SMC may exceed significantly, by a factor as much as  $\sim 10$ , the value derived for the Milky Way and other nearby galaxies by Grimm et al. (2003). Note that the analysis and interpretation of the SMC data in Grimm et al. (2003) was based on the star formation rate estimates obtained by Filipovic et al. (1998) from the supernovae rate.

### 5.3 The XLF shape

At the first glance the shape of the HMXB XLF obtained by XMM-Newton appears to be more complex than a single slope  $N(> L) \propto L^{-0.6}$  power law in the entire  $\sim 10^{34} - 10^{38}$  erg/sec luminosity range.

The maximum likelihood fit to the bright end of the distribution ( $L_X > 2 \cdot 10^{35}$  erg/s) with a power law results in the best fit value of the cumulative slope  $\alpha = 0.74^{+0.22}_{-0.19}$  which is consistent with the slope of 0.6. This is also confirmed by the Kolmogorov-Smirnov (K-S) test which gives probability of  $\sim 17\%$ . Thus, the bright end of the XLF is consistent with the universal HMXB XLF. This conclusion is further confirmed by the ASCA XLF containing by a factor of  $\sim 3$  more sources.

At low luminosities the uncertainties of HMXB identification procedure become of importance and we consider the upper and lower limits of the XLF separately. The upper limit on the XLF (the upper histogram in Fig. 5) is consistent with a single slope power law in the luminos-

ity range  $L_X > 10^{34}$  erg/s with the K-S test probability of  $\sim 75\%$  and the best fit value of the slope  $\alpha = 0.5 \pm 0.08$ . For the lower histogram in Fig. 5 (luminosity distribution of reliable HMXB candidates) we obtain best fit slope of  $\alpha = 0.37 \pm 0.08$  in the full luminosity range. The observed distribution, is consistent with a single slope power law – the K-S test probability is  $\approx 33\%$ . A power law approximation in the  $10^{34} - 2 \cdot 10^{35}$  erg/sec luminosity range gives the best fit slope of  $\alpha \approx 0.13^{+0.30}_{-0.13}$ .

Thus, the behavior of the XLF in the faint end is somewhat uncertain. However, based on the statistical arguments and the distribution of the optical magnitudes (see sec. 4.3 and 5.4), the majority of sources of uncertain nature are expected to be the result of chance coincidence. Therefore the lower histogram in Fig. 5 should better represent the true HMXB XLF and the flattening of the XLF in the faint end can be real. It can result from the “propeller” effect, as suggested by Shtykovskiy & Gilfanov (2005).

#### 5.4 Optical properties of HMXB candidates

The distribution of V-band magnitudes of the HMXB candidates is shown in Fig. 6. In the case of the likely HMXB candidates it shows bimodal structure with two peaks at  $m_V \approx 14.6$  and  $m_V \approx 15.5$ . To estimate the statistical significance of the observed bimodality, we perform a test based on the bootstrap method (Silverman 1981). The obtained value of significance is rather low and does not allow us to make a definite conclusion (with probability that the observed distribution is multimodal of 97%, i.e. significance slightly above  $2\sigma$ ).

The origin of this bimodality, if real, is not clear. It could correspond to Be/X-ray systems with main sequence and giant Be secondaries. However, this explanation is not satisfactory as it would require a rather narrow distributions of the optical companions over spectral classes.

The distribution of the  $m_V$  magnitudes of the uncertain HMXB candidates differs from those of likely candidates. This is consistent with expectations, that significant part of them should be a chance coincidences (see sec. 4.3).

#### 6 LOG(N)–LOG(S) DISTRIBUTION OF CXB SOURCES IN THE DIRECTION OF SMC

The log(N)–log(S) distributions of CXB sources, obtained after removal of likely HMXB candidates only and all HMXB candidates are shown in Fig. 7. We fit the resulting log(N)–log(S) distribution in the flux range  $F_X > 2 \cdot 10^{-14}$  erg  $\text{cm}^{-2} \text{ s}^{-1}$  with a power law model  $N(> S) = k(S/S_0)^{-\alpha}$ , where  $S_0 = 2 \cdot 10^{-14}$  erg/s/cm $^2$ . Best fit value of slope for the case with only likely HMXB candidates excluded is  $\alpha = 1.48 \pm 0.12$ . For the case with all the HMXB candidates excluded we obtain  $\alpha = 1.55 \pm 0.13$ .

We also compare the resulting log(N)–log(S) distributions in the flux range  $F_X > 2 \cdot 10^{-14}$  erg  $\text{cm}^{-2} \text{ s}^{-1}$  with CXB number counts obtained by Moretti et al (2003). The Kolmogorov-Smirnov test accepts their model giving probabilities  $\sim 96\%$  for the case with likely HMXB candidates excluded and  $\sim 76\%$  for the case with all the HMXB candidates excluded. The number of sources at flux  $2 \cdot 10^{-14}$  erg  $\text{cm}^{-2} \text{ s}^{-1}$  predicted by Moretti et al (2003),  $N = 178^{+96}_{-46}$ , is

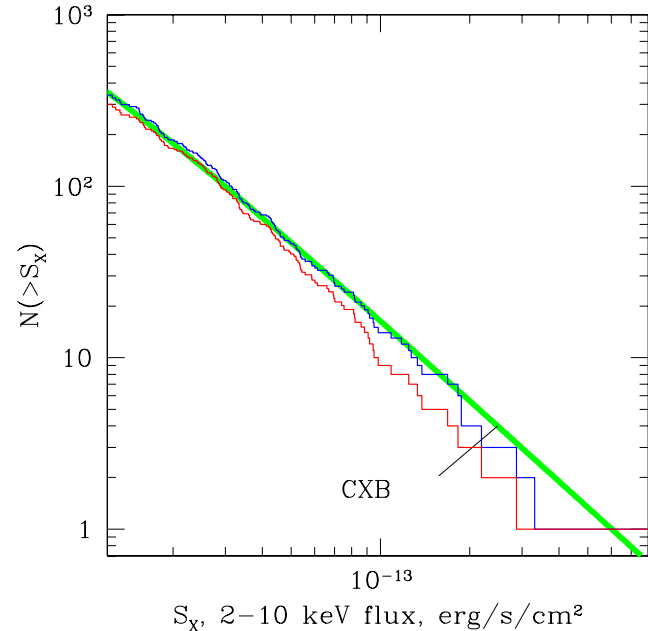


**Figure 7.** Cumulative logN–logS distribution of CXB sources, obtained after removal of all HMXB candidates (lower histogram) and only likely HMXB candidates (upper histogram). The solid line shows the CXB log(N)–log(S) distribution from Moretti et al (2003). The brightest source has flux  $S_X = 2.85 \cdot 10^{-12}$  erg/s/cm $^2$ .

also consistent with the observed numbers,  $N = 167 \pm 13$  and  $N = 186 \pm 14$  for the two above cases respectively.

Thus, the CXB log(N)–log(S) in the direction of the SMC is consistent both in the shape and the normalization with results of other CXB surveys.

#### 7 SUMMARY

Based on the archival data of XMM–Newton observations, we studied the population of point-like sources in the field of the SMC. The total area of the survey is  $\approx 1.5$  sq.degr. with the limiting sensitivity of  $\sim 10^{-14}$  erg/s/cm $^2$  (Fig.2), corresponding to the luminosity of  $\sim 2.3 \cdot 10^{33}$  erg/s at the SMC distance.

(i) Out of the 196 compact sources, detected in the 2–8 keV energy band,  $\sim 3/4$  are CXB sources, observed through the SMC (section 3.1, Fig.3).

(ii) Based on the stellar mass and the star formation rate of the SMC we demonstrate, that the majority of the intrinsic SMC sources, detected in the 2–8 keV band are high mass X-ray binaries (section 3).

(iii) The proximity of the SMC and adequate angular resolution of XMM–Newton make it possible to reliably filter out the sources, whose properties are inconsistent with HMXB nature. Based on the optical and infrared magnitudes and colors of the optical counterparts of the X-ray sources we identify 32 likely HMXB candidates (29 of which were previously known) and 18 sources of uncertain nature (section 4, Table 2). The remaining  $\sim 146$  sources, with a few exceptions, are background objects, constituting the resolved part of CXB. Their flux distribution is consistent

both in shape and normalisation with other determinations of the CXB log(N)–log(S) (section 6, Fig.7).

(iv) With these results we constrain lower and upper bounds of the luminosity distribution of HMXBs in the observed part of the SMC. We compare these with the extrapolation towards low luminosities of the universal luminosity function of HMXBs, derived by Grimm et al. (2003) (Fig. 5).

The observed number of HMXBs is consistent with the prediction based on SFR estimates derived from supernovae frequency and analysis of the stellar color-magnitude diagrams. If, on the contrary, the true value of the SFR is better represented by FIR,  $H_{\alpha}$  and UV based estimators, then the abundance of HMXBs in the SMC may significantly (by a factor of as much as  $\sim 10$ ) exceed the value derived for the Milky Way and other nearby galaxies (sections 3.3, 5).

The shape of the observed distribution at the bright end is consistent with the  $N(> L) \propto L^{-0.6}$  power law of the universal HMXB XLF. At the faint end,  $L_X \lesssim 2 \cdot 10^{35}$  erg/s, the upper limit of the luminosity function is consistent with the  $L^{-0.6}$  power law, while the lower limit is significantly flatter.

## 8 ACKNOWLEDGEMENTS

This research has made use of data obtained through the High Energy Astrophysics Science Archive Research Center Online Service, provided by the NASA/Goddard Space Flight Center. This publication has made use of data products from the Two Micron All Sky Survey, Guide Star Catalogue-II. PS acknowledges the support of European Association for Research in Astronomy (MEST-CT-2004-504604 Marie Curie - EARA EST fellowship at Max-Planck-Institute for Astrophysics). PS also acknowledges a partial support from the President of the Russian Federation grant SS-2083.2003.2.

## REFERENCES

Bell E., de Jong R., 2001, ApJ, 550, 212  
 Bell E., 2003, ApJ, 586, 794  
 M.J. Coe, W.R.T. Edge, J.L. Galache, V.A. McBride, 2004, astro-ph/0410074  
 Corbet R.H.D., 1986, MNRAS, 220, 1047  
 Cutri R. M., Skrutskie M. F., van Dyk S., Beichman C. A., Carpenter J. M., Chester T., Cambresy L. et al., 2003, yCat, 224  
 de Vaucouleurs G. et al., 1991, Third Reference Catalog of Bright Galaxies. Springer-Verlag (RC3)  
 Edge W. R. T., Coe M. J., 2003, MNRAS, 338, 428  
 Edge W. R. T., Coe M. J., Galache J. L., McBride V. A., Corbet R. H. D., Markwardt C. B., Laycock S., 2004, MNRAS, 353, 1286  
 Evans C.J., Howarth I.D., Irwin M.J., Burnley A.W., Harries T.J., 2004, MNRAS, 353, 601  
 Filipovic M. et al., 1998, A&A Auppl., 127, 119  
 Filipovic M. D., Pietsch W., Haberl F., 2000, A&A, 361, 823  
 Gehrz R. D., Hackwell J. A., Jones T. W., 1974, ApJ, 191, 675  
 Gilfanov M., 2004, MNRAS, 349, 146  
 Grimm, H.-J., Gilfanov, M.R., Sunyaev, R.A. 2003, MNRAS, 339, 793  
 Haberl F., Pietsch W., 2004, A&A, 414, 667  
 Haberl F., Pietsch W., Schartel N., Rodriguez P., Corbet R. H. D., 2004, A&A, 420L, 19  
 Harris J., Zaritsky D., 2004, AJ, 127, 1531  
 Helou et al., 1985, ApJ, 298, L7  
 Kennicutt R.C. Jr. 1991, in: Haynes R.F. & Milne D.K. (eds.) Proc. IAU Symp. 148, The Magellanic Clouds, Reidel, Dordrecht, p.139  
 Kennicutt R.C. Jr., 1998, ARA&A, 36, 189  
 Kennicutt R.C. Jr., Bresolin F., Bomans D.J., Bothun G.D., Thompson I.B., 1995, AJ, 109, 594  
 Lamb R. C., Fox D. W., Macomb D. J., Prince T. A., 2002, ApJ, 574, 29  
 Majid W. A., Lamb R. C., Macomb D. J., 2004, ApJ, 609, 133  
 Massey P., 2002, yCat, 2236, 0  
 McGlynn T., Scollick K., White N., SkyView: The Multi-Wavelength Sky on the Internet, McLean, B.J. et al., New Horizons from Multi-Wavelength Sky Surveys, Kluwer Academic Publishers, 1996, IAU Symposium No. 179, p465.  
 Meyssonnier N., Azzopardi M., 1993, A&AS, 102, 451  
 Monet D.G., Levine S.E., Canzian B., Ables H.D., Bird A.R., Dahn C.C., Guetter H.H. et al., 2003, AJ, 125, 984  
 Moretti A., Campana S., Lazzati D., Tagliaferri G., 2003, ApJ, 588, 696  
 Morrison J. E., McLean B., GSC-Catalog Construction Team, II, 2001, DDA, 32.0603  
 Negueruela I., 1998, A&A, 338, 505  
 Shtykovskiy P., Gilfanov M., 2005, A&A, 431, 597  
 Silverman B.W., 1981, J.R.Statist.Soc.B, 43, 97  
 Udalski A., Szymanski M., Kubiak M. et al., 1998, yCatp005004802U  
 van Paradijs, J. & McClintock J.E., 1995, X-ray Binaries, Cambridge Univ.Press, p.58  
 Vangioni-Flam E. et al., 1980, A&A, 90, 73  
 Westerlund B., “The Magellanic Clouds”, Cambridge Univ.Press, 1997  
 Wilke K., Klaas U., Lemke D. et al., 2004, A&A, 414, 69  
 Yokogawa J., Imanishi K., Tsujimoto M., Nishiuchi M., Koyama K., Nagase F., Corbet R.H.D., 2000, ApJS, 128, 491  
 Yokogawa J., Imanishi K., Tsujimoto M., Koyama K., Nishiuchi M., 2003, PASJ, 55, 161  
 Zaritsky D., Harris J., Thompson I.B., Grebel E.K., Massey P., 2002, AJ, 123, 855

## APPENDIX A: CROSS-CORELLATION OF TWO CATALOGUES

Below we consider the problem of cross-corellation of two catalogs (e.g. of the list of detected X-ray sources and an optical catalogue). More specifically we concentrated on the case when only a fraction of X-ray sources has true optical counterparts in the optical catalogue and when the probability of chance coincidences is not negligible. In this case, the matches of X-ray sources with optical sources will include real optical counterparts and chance coincidences. We consider the behavior of the growth curves – the dependence of

the number of matches on the search radius. We show that using different dependences of the number of true matches and chance coincidences on the search radius, it is possible to estimate the number of true optical counterparts.

### A1 Case of constant density of optical stars

The number of X-ray sources with optical matches inside radius  $r$  depends on the number of X-ray sources which have true optical counterpart inside  $r$  and number of chance coincidences of X-ray sources with field stars:

$$N_{Xmatch} = N(1 - e^{-\rho\pi r^2}) + M e^{-\rho\pi r^2} \int_0^r \phi(r') dr', \quad (A1)$$

where  $N$  - total number of X-ray sources,  $M$  - number of X-ray sources with true optical counterparts,  $\rho$  - density of optical field stars (i.e. excluding the true optical counterparts) and  $\phi(r)$  is the distribution of distances between X-ray sources and their optical counterparts. The first term in the above equation is a number of chance coincidences, i.e. number of X-ray sources which have at least one field star inside its search radius. The second term corresponds to number of true matches falling inside search radius  $r$ . The exponent in this term excludes cases when both true optical counterpart and chance coincidence with field stars are present, as such matches were already taken into account in the first term. Assuming that all X-ray sources have the same positional error  $\sigma$  (hence  $\phi(r) = r/\sigma^2 \cdot e^{-r^2/2\sigma^2}$ ), we can rewrite this equation in the following way:

$$N_{Xmatch} = N(1 - e^{-\rho\pi r^2}) + M e^{-\rho\pi r^2} (1 - e^{-r^2/2\sigma^2}). \quad (A2)$$

Fitting the curve  $N_{Xmatch}(r)$  with this formula one can determine the number of X-ray sources with true optical matches, surface density of optical stars  $\rho$  and error on the source positions.

### A2 Non-constant surface density of optical stars

In a real situation, the density of optical stars  $\rho$  varies from field to field and even from source to source. This can lead to significant deviations of  $N_{Xmatch}(r)$  curve behaviour from the eq. A2. There is no obvious way to overcome this problem completely. However, the density variations could be partially taken into account by replacing the mean density of optical objects in the first term of eq. A2 by the local densities of optical objects around each individual X-ray source. The first term in this case, of course, should be replaced by the corresponding sum over all X-ray sources. The density  $\rho$  in the second term, however, cannot be straightforwardly calculated because it is related to X-ray sources with true optical counterparts, which we do not know a priori. Thus, modifying the first term in equation A2 we obtain:

$$N_{Xmatch} = \sum_{i=1}^N (1 - e^{-\rho_i \pi r^2}) + M e^{-\rho\pi r^2} (1 - e^{-r^2/2\sigma^2}). \quad (A3)$$

The local densities  $\rho_i$  of optical objects should be calculated individually for each X-ray source. The areas over which these densities are calculated must be large enough to minimize the relative contribution of the true optical counterparts and Poissonian errors. Density  $\rho$  corresponds now to

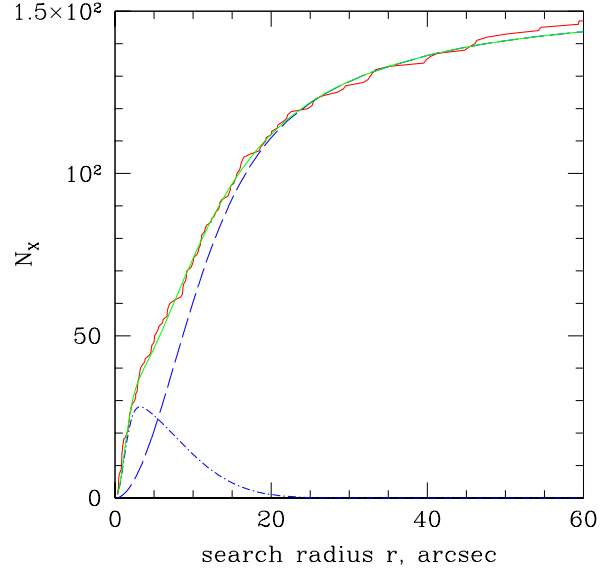


**Figure A1.** The number of X-ray sources with an optical match as a function of search radius and its approximation with eq. A3. The individual components of this equation corresponding to spurious matches with field stars and true optical counterparts (which don't have simultaneous spurious matches) are shown with dashed and dot-dashed lines respectively.

the mean density of optical objects near X-ray sources which have true optical counterparts.

Fit parameters are the number of X-ray sources with true optical matches  $M$ , the value of positional error  $\sigma$  and the mean density of optical objects  $\rho$ . Fitting the  $N_{Xmatch}(r)$  curve using real list of XMM sources and optical sources from the MCPS catalogue we obtain the best fit value for the total number of sources with true optical counterpart in our sample is  $\sim 31$ , surprisingly close to the number of our likely HMXB candidates (see Fig. A1). Best fit value of positional error,  $\sigma \approx 1.2''$ , also agrees with typical values for X-ray sources from our list ranging from  $\approx 0''$  to  $\approx 2''$ . We note also, that from the eq. A3 it follows that subtracting the first sum from  $N_{Xmatch}$  curve and multiplying the remaining part by  $e^{\rho\pi r^2}$ , we can obtain the dependence of the number of true counterparts among optical matches on the search radius. The resulting curve is shown on Fig. A2. It is clear from this figure, that almost all true optical counterparts of X-ray sources will be detected with the search radius of  $4''$  used in our HMXB identification procedure.

### A3 Account for spread in distribution of positional uncertainties

The deviation of positional errors distribution from the delta function together with the astrometric uncertainty can also modify  $N_{Xmatch}(r)$  curve. With the spread in positional errors accounted for, the equation A3 becomes:

$$N_{Xmatch} = \sum_i (1 - e^{-\rho_i \pi r^2}) + M e^{-\rho\pi r^2}. \quad (A4)$$

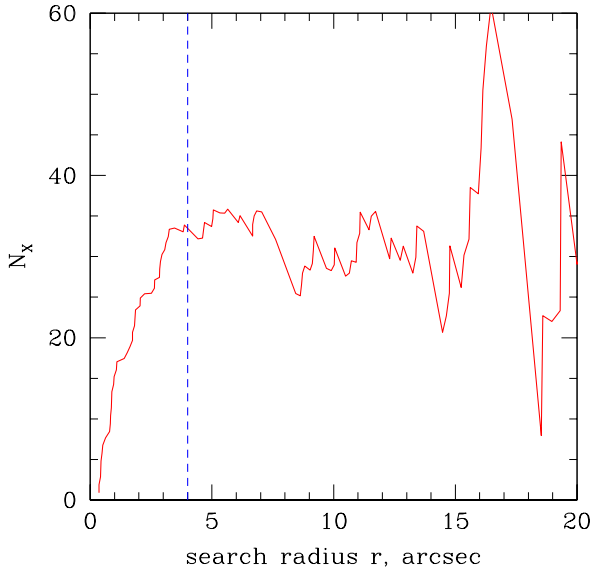


**Figure A2.** Number of true matches as a function of radius estimated using eq. A3 (see A2). The vertical dashed line shows the search radius of 4 arcsec. It is clear from this figure, that almost all true optical counterparts of X-ray sources fall within the chosen search radius.

$$\cdot \int \int \phi(r', \sigma) g(\sigma) d\sigma dr',$$

where  $\phi(r, \sigma) \propto re^{-r^2/2\sigma^2}$  is the (Gaussian) distribution of distances between the X-ray and optical sources for given  $\sigma$  and  $g(\sigma)$  is a distribution of positional uncertainties of X-ray sources. To show that such a spread will not significantly change our results, we assumed that errors distribution follows the power law  $g(\sigma) \propto \sigma^\alpha$  between  $\sigma = 0.2''$  and  $2.3''$ . In this case the free fit parameters are the number of X-ray sources with true counterparts  $M$ , optical sources density  $\rho$  and slope  $\alpha$ .

Fitting our curve with this formula we obtained the best fit value  $M=34$ , which also agrees well with the number of our likely HMXB candidates.